

## Article

# Studies on Insertion/Deletion Residues for Functional Analysis and Improved Amination Activity in *Meso*-DAPDH from *Corynebacterium glutamicum*

Yaning Zhang <sup>†</sup>, Jiaying Hao <sup>†</sup>, Yongjun Cao, Wenjun Zhao, Hankun Liu, Xiuzhen Gao <sup>\*†</sup>  and Qinyuan Ma <sup>\*</sup>

School of Life Science and Medicine, Shandong University of Technology, Zibo 255000, China; zyn400651@hotmail.com (Y.Z.); hjy19811718971@hotmail.com (J.H.); cyj2816443450@hotmail.com (Y.C.); azhaowj123@hotmail.com (W.Z.); aliuhk@hotmail.com (H.L.)

<sup>\*</sup> Correspondence: gaoxz@sdut.edu.cn (X.G.); qyma@sdut.edu.cn (Q.M.)

<sup>†</sup> These authors contributed equally to this work.

**Abstract:** *Meso*-diaminopimelate dehydrogenase (*meso*-DAPDH) from *Corynebacterium glutamicum* ATCC13032 (CgDAPDH) is a type I *meso*-DAPDH that shows obvious preference toward *meso*-diaminopimelate (*meso*-DAP) and exhibits almost no amination activity toward 2-keto acids. There are seven distinct conserved insertions and deletions (indels) between type I and type II *meso*-DAPDH. The current functional analysis of indels is not comprehensive in *meso*-DAPDH. Continuing from our previous work on these indels, we first examined the functions of the other indels shown as insertion residues in type I CgDAPDH. Alanine mutations in M216, T240, K289, and Q290 lost at least 40% of their activity, highlighting the importance of these four sites in CgDAPDH. Molecular dynamic analysis indicated that the four non-active sites altered the dynamic network of interactions within the protein. Subsequently, these four sites together with the previously identified indel-related residues R180, L176, and H193 were targeted by site-saturation mutagenesis to improve the amination ability of CgDAPDH toward pyruvic acid. The most significant improvement was observed with the mutant CgL176R, which showed a six-fold increase toward pyruvic acid in  $k_{cat}/K_m$  compared to wild-type CgDAPDH. Overall, our study provides new hotspots and ideas for the subsequent protein engineering of CgDAPDH, which may also be applied to other *meso*-DAPDHs.

**Keywords:** indels; *meso*-diaminopimelate dehydrogenase; functional analysis; molecular dynamic simulation; substrate spectrum modification; reduction amination



**Citation:** Zhang, Y.; Hao, J.; Cao, Y.; Zhao, W.; Liu, H.; Gao, X.; Ma, Q. Studies on Insertion/Deletion Residues for Functional Analysis and Improved Amination Activity in *Meso*-DAPDH from *Corynebacterium glutamicum*. *Catalysts* **2024**, *14*, 220. <https://doi.org/10.3390/catal14040220>

Academic Editor: Per Berglund

Received: 20 February 2024

Revised: 16 March 2024

Accepted: 19 March 2024

Published: 22 March 2024



**Copyright:** © 2024 by the authors. Licensee MDPI, Basel, Switzerland. This article is an open access article distributed under the terms and conditions of the Creative Commons Attribution (CC BY) license (<https://creativecommons.org/licenses/by/4.0/>).

## 1. Introduction

*Meso*-diaminopimelate dehydrogenase (*meso*-DAPDH; EC 1.4.1.16) catalyzes the reversible oxidative deamination of *meso*-diaminopimelate (*meso*-DAP) with high D-stereoselectivity [1]. *Meso*-DAPDH from *Corynebacterium glutamicum* ATCC13032 (Cg-DAPDH) was the first *meso*-DAPDH to be characterized [2,3] and have its 3D structure determined by different methods and ligands [4]. However, to a great extent, CgDAPDH is unable to catalyze the reversible amination reactions of 2-keto acids into other D-amino acids [5]. In 2012, *meso*-DAPDH from *Symbiobacterium thermophilum* IAM14863 (StDAPDH) was characterized as the first wild-type (WT) *meso*-DAPDH that could effectively catalyze the reductive reaction from 2-keto acids, which indicated that natural *meso*-DAPDH can catalyze the one-step amination of 2-keto acids to generate D-amino acids [6].

Subsequently, divergent evolution of the *meso*-DAPDH family has been proposed [7]. *Meso*-DAPDH enzymes are now divided into two types, with type I showing highly preferable activity toward *meso*-DAP and type II exhibiting significant reversible amination activity with a broad substrate specificity. The average length of type I *meso*-DAPDHs is approximately 327 amino acids, whereas the average length of type II *meso*-DAPDHs is

299 amino acids. Insertions and deletions (indels) are highly conserved within each type (Figure 1a), and the two types exhibit distinct patterns of indel distribution [7].

Indels in protein sequences can lead to a series of structural changes [8]. The primary driving forces underlying the divergent evolution of enzyme families involve indels that affect substantial fragments and substitutions that occur at specific amino acid sites [9]. Site-directed mutations result in a side-chain change that tends to have a local effect and usually has little effect on the overall structure of the protein. In contrast, indels alter the length of the protein skeleton, potentially leading to significant changes in the arrangement and orientation of the domains, which can have a global impact on the protein structure [8]. By repositioning the protein skeleton and nearby side chains, indels can lead to structural changes that may affect enzyme specificity and activity. For example, Yan et al. gradually inserted amino acids into the loop 7 region near the active site of phosphotriesterase and observed a 16-fold improvement in the catalytic efficiency of the screened optimal mutant [10]. In addition, indels at the interaction interfaces of protein subunits can affect the stability or substrate specificity of the protein [11]. For example, the single subunit of phosphonate monoester hydrolase was found to maintain enzyme stability through its interaction with the C-terminal region. However, truncation of the C-terminal region resulted in virtually undetectable enzyme activity [12]. Finally, indels can contribute to the evolution of protein families, resulting in proteins with diverse functions. For example, apicomplexan lactate dehydrogenases (LDHs), which evolved from malate dehydrogenase (MDH), prefer pyruvic acid as their substrate, while MDH uses oxaloacetic acid. Theobald et al. confirmed that these differences in substrate specificity were due to the loop inserted between amino acids 102 and 109 of LDH [13].

Multiple sequence alignment of type I and type II revealed seven distinct and conserved indels. The longest of these sequences occurs in the form of a loop (177E-192Q) in the tertiary structure, which is referred to as the 'indel loop'. Previous studies found that the indel loop played a crucial role in CgDAPDH catalysis [14]. The mutation of R180A within the loop has been shown to lead to an almost complete loss of activity. The hydrogen bond interactions formed between R180 and E262 maintain the correct conformation of the catalytic cavity and the catalytic H152 residue. In addition, the indel loop forms a closed hydrogen bond network with the upstream L176 and downstream H193 residues, which stabilizes the hydrogen bond network formed by the amino acid side chains throughout the entire protein. These findings highlight the importance of the indel loop in CgDAPDH catalysis.

In addition, six short indels composed of 1–4 amino acids have been identified, although their functions remain unclear (Figure 1b). Furthermore, at present, enhancement of the amination activity of CgDAPDH through protein engineering is limited by the ability to identify and select suitable hotspots, especially non-active sites. Therefore, in this study, using CgDAPDH as a template, the remaining indels occurring in type I enzymes as insertion residues were mutated to alanine, and their roles in CgDAPDH catalysis were identified (Figure 1c). Then, the key non-active sites located on the indels and their flanks were set as hotspots in order to improve the amination activity of CgDAPDH toward pyruvic acid by site-directed saturation mutagenesis.

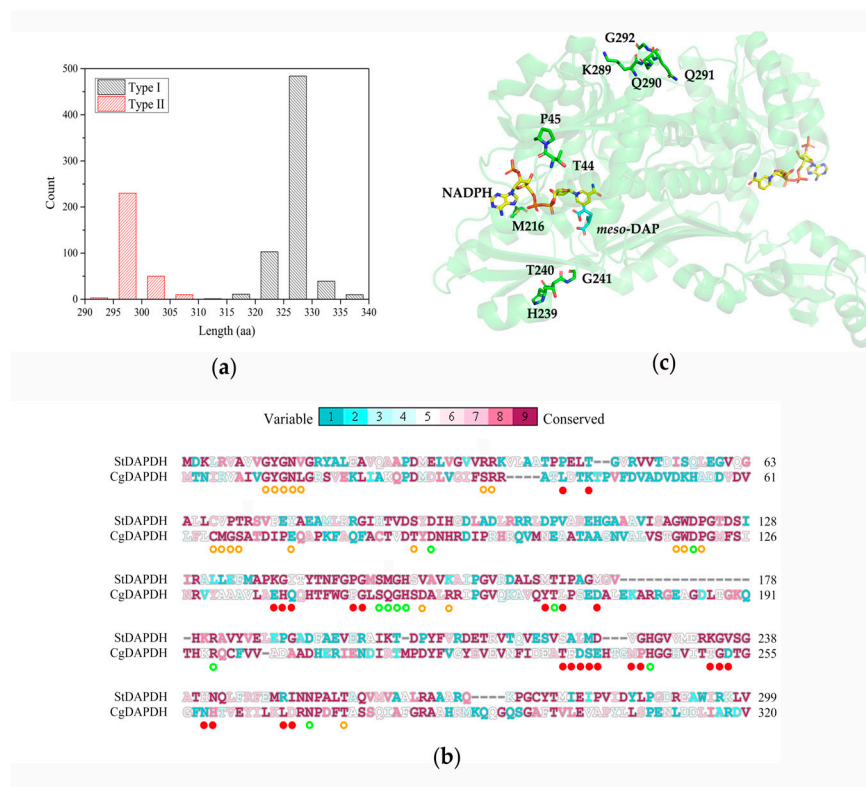


**Figure 1.** Length and ConSurf analysis of two types of *meso*-DAPDHs: (a) distribution of amino acid sequence lengths of *meso*-DAPDHs, and (b) multiple sequence alignment between subtypes of DAPDH presented as StDAPDH and CgDAPDH. The predicted substrate-binding residues of StDAPDH are shown as green circles, and NADP<sup>+</sup>-binding residues are shown in orange. Residues involved in multimerization are shown as red dots. On the conservation scale, grade 1 represents the most highly variable amino acid positions (turquoise), and grade 9 represents the most highly conserved positions (maroon). These figures have been modified and referenced from our previous work [7,14], (c) locations of the residues studied in this work (shown as sticks).

## 2. Results

### 2.1. Screening of Key Insertion Residues in CgDAPDH by Alanine Mutagenesis

Based on our previous study on the indel loop, we targeted the amino acid residues located on the indels, which are shown as insertion residues occurring in type I enzymes, to determine their role in CgDAPDH catalysis. Because alanine has a non-bulky, chemically inert, methyl functional group, alanine scanning mutagenesis is a common method used to analyze the function of specific amino acid residues in proteins. Here, ten alanine mutants of CgDAPDH were constructed in total, and their kinetic constants were determined using *meso*-DAP as the substrate (Table 1). We found that the catalytic efficiencies of all alanine mutants were significantly reduced. The  $K_m$  value of all alanine mutants increased by 105% to 250% compared to WT CgDAPDH. Although slight decreases in the  $k_{cat}$  value of T240A, G241A, K289A, and Q291A were observed compared to WT CgDAPDH (ranging from 92% to 97%), these changes were not significant. The  $k_{cat}$  values of H239A and G292A were higher than those of the WT, but the differences were very small and almost negligible. The  $k_{cat}$  values of T44A, P45A, and M216A were significantly increased and were found to be 1.48, 1.49, and 1.72 higher than the WT values, respectively. Interestingly, the higher  $K_m$  values were found to reduce the catalytic efficiency of the three mutants. Specifically, the  $K_m$  value of M216A was 2.5 times higher than the WT value. Our findings suggested that the decrease in catalytic efficiency was due to the increase in  $K_m$ , which affected substrate affinity. Compared with WT CgDAPDH, the catalytic efficiency of M216A, T240A, and K289A on *meso*-DAP was reduced by approximately 30%, while a decrease

of approximately 50% was observed with Q290A. The other CgDAPDH alanine mutants displayed less significant effects. Together, these results indicated that the indel residues M216, T240, K289, and Q290, which are also non-active sites (Figure 1c), were significantly more important than the other six insertion residues for the catalysis of CgDAPDH.

**Table 1.** Kinetic parameters of *meso*-DAP in WT CgDAPDH and its alanine mutants.

Enzyme	$K_m$ (mM)	$k_{cat}$ (s <sup>-1</sup> )	$k_{cat}/K_m$ (s <sup>-1</sup> ·mM <sup>-1</sup> )	Relative $k_{cat}/K_m$
CgDAPDH	0.57 ± 0.06	100.13 ± 3.20	176 ± 24	1.00
T44A	0.93 ± 0.08	147.80 ± 5.00	159 ± 19	0.90
P45A	0.87 ± 0.08	148.71 ± 5.30	171 ± 22	0.97
M216A	1.45 ± 0.10	172.24 ± 6.10	119 ± 12	0.68
H239A	0.65 ± 0.05	102.21 ± 2.70	157 ± 16	0.90
T240A	0.86 ± 0.06	97.87 ± 3.10	114 ± 12	0.65
G241A	0.63 ± 0.08	93.91 ± 5.80	149 ± 28	0.85
K289A	0.77 ± 0.06	92.11 ± 2.70	120 ± 13	0.68
Q290A	1.03 ± 0.09	90.36 ± 4.00	88 ± 12	0.50
Q291A	0.60 ± 0.04	95.04 ± 2.10	158 ± 14	0.90
G292A	0.74 ± 0.04	103.53 ± 2.20	140 ± 11	0.80

## 2.2. Molecular Dynamic (MD) Simulations for Alanine Mutants

In order to elucidate the possible mechanisms through which these insertion residues affected CgDAPDH catalysis, we performed 50 ns MD simulations with WT CgDAPDH and its alanine mutants M216A, T240A, K289A, and Q290A, which displayed reduced catalytic efficiency at 298 K. Figure S1 shows variations in the root-mean-square deviation (RMSD), which indicate that CgDAPDH and the alanine mutant complexes were dynamically equilibrated after 40 ns.

Proteins are intrinsically dynamic [15], and both the structure and function of a protein relies on its dynamics. Different regions of the protein structure exhibit highly correlated or anti-correlated motion, reflecting the same or opposite direction of motion, respectively. These related residues can form a dynamic cross-correlation network, through which information can be transmitted to link, for example, the binding of a molecule at one site on a protein to changes in the local structure elsewhere in the protein [16]. The dynamic cross-correlation map (DCCM) is an excellent tool for analyzing the associated movement of amino acid residues in proteins, especially on the C $\alpha$  atom [17]. Here, we created a DCCM using the last 10 ns of the MD simulation trajectory of WT CgDAPDH and its alanine mutants. The DCCM analysis revealed that four mutations significantly changed the motility correlation between amino acid residues (Figure 2). The DCCM of M216A identified a new negative correlation between the loop at M216 after mutation and the amino acids at positions K20-A80 of M216A. In addition, a novel negative correlation was found between the amino acids L170-R180 and the catalytic-related residues in the D90 and D120 loops (Figure 2a,b). The DCCM of T240A revealed a new negative correlation between the amino acids Q150-P160 and V200-E210 with the loop containing the catalytic-related residues D90 and D120 (Figure 2c). And K289A and Q290A exhibited similar DCCMs (Figure 2d,e). These two mutants lacked the presence of an  $\alpha$ -helix located at A280-G295 along with any correlations between loops in which catalytic-related residues (D90/D120/H245) were situated when compared to WT CgDAPDH. Although M216, T240, K289, and Q290 are non-active sites outside of the enzyme substrate-binding domain, the dynamic interaction network of amino acids affected the relative movement of catalytic active sites after mutation, resulting in a loss of activity.

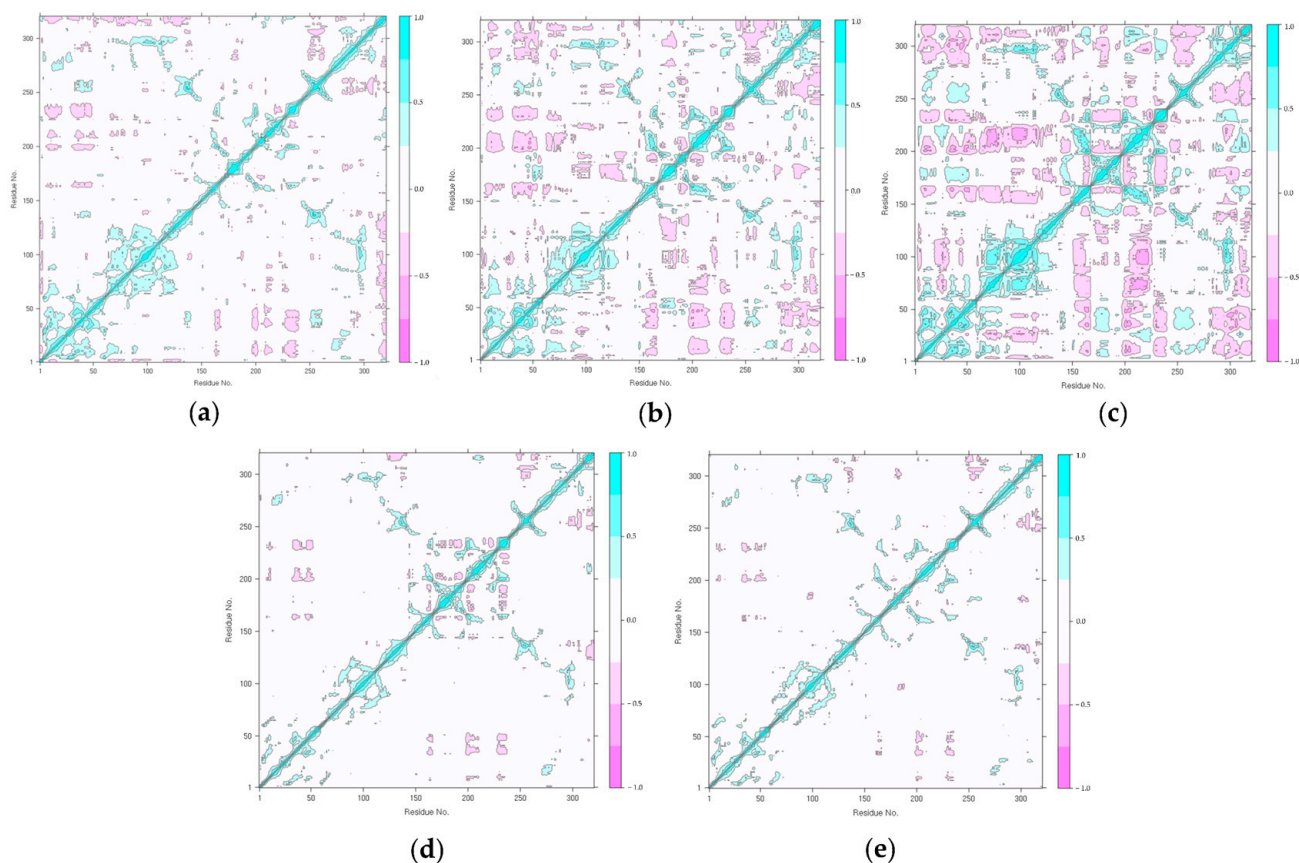


**Figure 2.** DCCM analysis within WT CgDAPDH and its mutants: (a) CgDAPDH, (b) M216A, (c) T240A, (d) K289A, and (e) Q290A.

Next, we compared the binding free energy of WT CgDAPDH and its alanine mutants on *meso*-DAP and found that the binding free energies of M216A, T240A, K289A, and Q290A were increased by 17.57%, 24.43%, 12.91%, and 37.83%, respectively, compared to WT CgDAPDH (Figure S2). Indeed, WT CgDAPDH demonstrated the lowest energy requirement for substrate binding, indicating its superior stability in the bound state with *meso*-DAP. Among the four mutants, Q290A had the highest binding energy, which was consistent with our experimental results. The catalytic efficiency of Q290A for *meso*-DAP was the lowest among the four mutants.

The structures of CgDAPDH and its mutants with *meso*-DAP were clustered using the last 10 ns of the MD simulation trajectory. The catalytic pocket size of the structures with the highest number of clusters was subsequently analyzed (Figure 3). As depicted in Figure 3a, all the mutants had larger substrate-binding pockets than WT CgDAPDH. Previous studies have suggested that larger substrate-binding pockets may discourage alanine mutants from stabilizing an appropriate near-attack conformation [18,19]. Taken together, the binding energy between the mutants and *meso*-DAP increased, resulting in unstable binding of the mutants to the substrate. Furthermore, the alanine mutations led to changes in the morphology of the substrate pocket. These factors may contribute to the decreased catalytic efficiency observed in the alanine mutants.

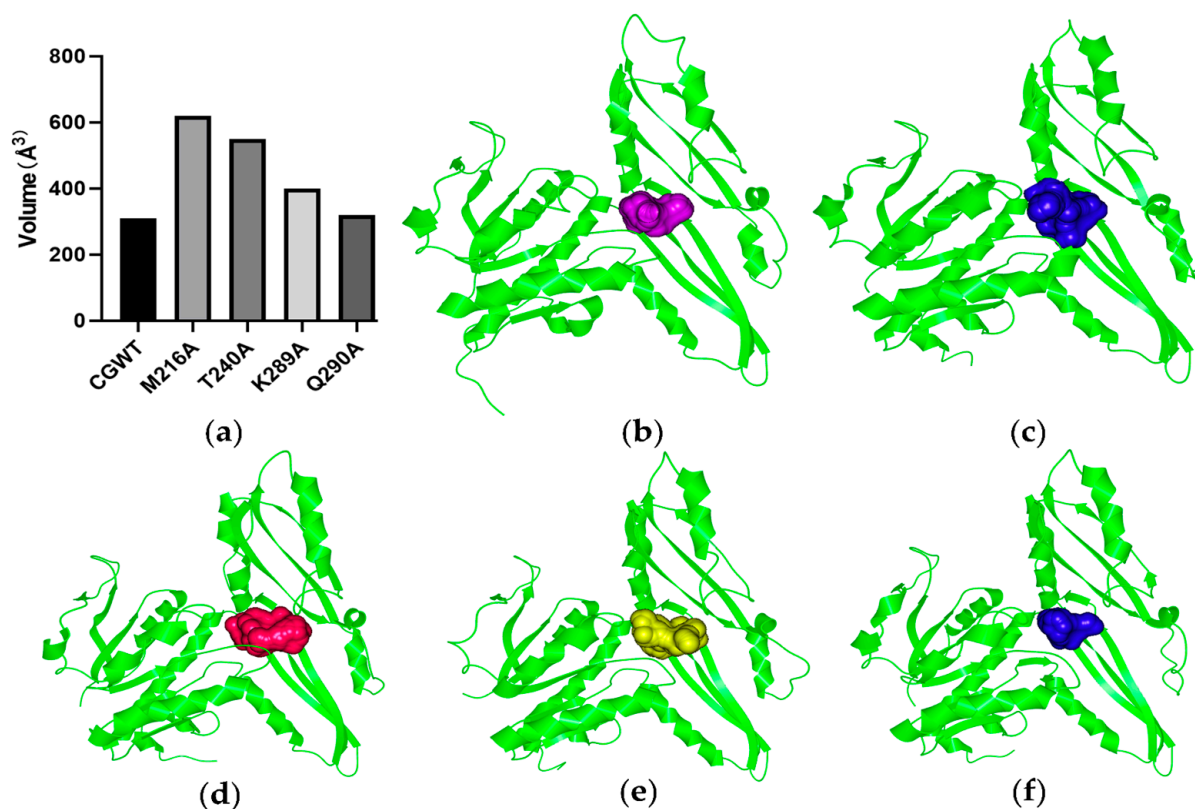


**Figure 3.** Comparison of the substrate-binding pocket between CgDAPDH and its mutants. (a) Substrate-binding pocket size of CgDAPDH and its mutants. (b–f) The morphology of the substrate-binding pocket of (b) CgDAPDH, (c) M216A, (d) T240A, (e) K289A, and (f) Q290A.

### 2.3. Protein Engineering of CgDAPDH to Improve Its Amination toward Pyruvic Acid

CgDAPDH, as the representative enzyme of type I *meso*-DAPDH, has almost no catalytic capacity for reductive amination [5,7]. We previously identified the insertion residue R180 located in the indel loop and the flanked residues L176 and H193 as key residues for CgDAPDH [14]. Thus, in the current study, we selected seven key residues including L176, R180, H193, M216, T240, K289, and Q290 as hotspots for protein engineering of CgDAPDH aimed at improving its amination ability, all of which are non-active sites. The seven site-saturation mutant libraries were screened by measuring changes in the optical density (OD) of nicotinamide adenine dinucleotide phosphate (NADPH) before and after the reaction. Beneficial mutants with higher activity toward pyruvic acid than WT CgDAPDH were then purified, and their specific activities toward pyruvic acid were determined in the second-round screening (Figure S3).

The mutant libraries of R180, M216, T240, K289, and Q290 did not lead to increased specific activity. Surprisingly, three mutants from library L176X and H193X displayed enzyme activities that were 3.6-fold, 2-fold, and 1.6-fold higher than those of WT CgDAPDH. These mutants were sequenced as L176R, L176M, and H193V. Subsequently, the kinetic parameters of pyruvic acid in the WT and mutants were determined (Table 2). L176M and H193V showed similar catalytic efficiency as the WT. L176R showed the highest catalytic efficiency, which was 6-fold higher than that of CgDAPDH. The  $K_m$  value of L176R was found to be reduced by 1.9 times compared to that of CgDAPDH, suggesting that the substrate affinity was improved in the L176R mutant, while the significant 2.5-fold increase in the  $k_{cat}$  value may account for the enhanced catalytic efficiency observed in L176R.

**Table 2.** Kinetic parameters of pyruvic acid in WT CgDAPDH and the positive mutants.

Enzyme	$K_m$ (mM)	$k_{cat}$ (s <sup>-1</sup> )	$k_{cat}/K_m$ (s <sup>-1</sup> ·mM <sup>-1</sup> )	Relative $k_{cat}/K_m$
CgDAPDH	17.5 ± 1.5	0.2 ± 0.01	0.01 ± 0.002	1.0
L176R	9 ± 0.5	0.5 ± 0.01	0.06 ± 0.004	6.0
L176M	15.5 ± 1.2	0.2 ± 0.01	0.01 ± 0.002	1.0
H193V	23 ± 3	0.3 ± 0.02	0.01 ± 0.003	1.0

#### 2.4. MD Simulation Analysis of Variant L176R

Mutant L176R exhibited the most significant improvements in amination toward pyruvic acid. Thus, we next sought to elucidate the potential mechanism mediating the increased activity of L176R toward pyruvic acid by performing 100 ns MD simulations of CgDAPDH and the L176R variant at 298 K. RMSD analysis of the MD trajectories revealed that the L176R protein was more stable than CgDAPDH during the whole simulation (Figure 4a). The RMSD values of the substrate movement indicated that the RMSD value of pyruvic acid in mutant L176R remained stable at 2.37 Å, which was more stable than that observed in CgDAPDH (Figure 4b). Catalytic attack of hydride can occur when the distance between the cofactor C4 atom and the carbonyl carbon atom of the substrate is less than 4.5 Å [20,21].  $C_{\text{substrate}} - C4_{\text{NADPH}} < 4.5$  Å were defined as ‘catalytic’ conformations. As shown in Figure 4c, the substrate in CgDAPDH completely exceeded the ‘catalytic’ conformations. However, the proportions of such conformations in L176R were 42% during the last 20 ns MD simulations, suggesting that the active pocket of L176R was better at stabilizing the substrate in the ‘catalytic’ conformation. These findings are consistent with the higher  $k_{cat}$  values of L176R. Together, our results suggested that L176R possesses a stable conformation that is favorable for catalysis.

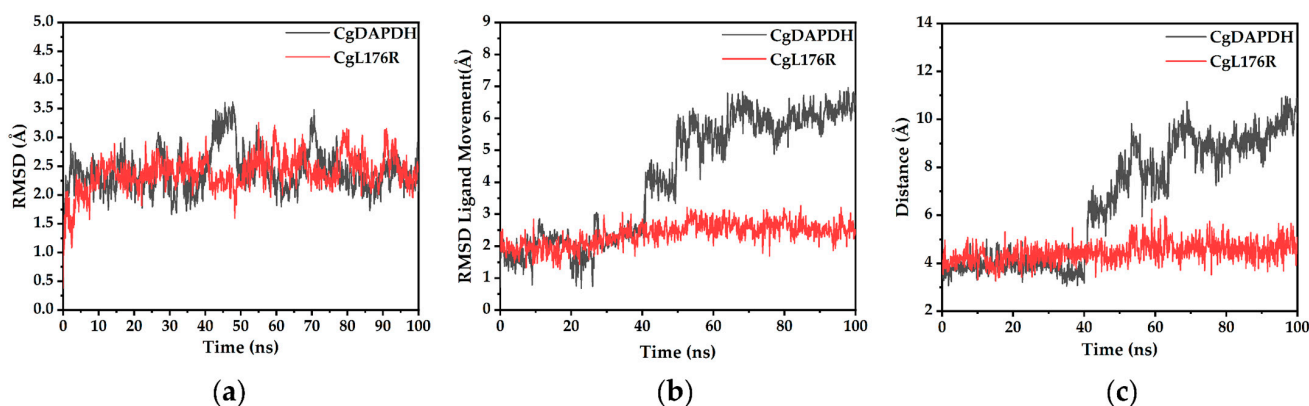


**Figure 4.** MD analysis: (a) RMSD analysis of the C $\alpha$  atom for WT CgDAPDH and L176R in the complex with pyruvic acid, (b) RMSD analysis of ligand movement for WT CgDAPDH and L176R and (c) distance analysis of the ‘catalytic’ conformation for WT CgDAPDH and L176R.

Subsequently, the hydrogen bond interactions formed between the amino acid residues and pyruvic acid were analyzed in the final 20 ns of the MD trajectory (Figure 5). Hydrogen bonds were present between S149, T169, and H244, and pyruvic acid with an occupancy rate of 71%, 94%, and 86%, respectively (Figure 5a). The resulting hydrogen bond interaction network anchored the substrate in an inappropriate catalytic position, which caused the distance between the pyruvic acid and NADPH to exceed the interaction range (Figure 5b). In contrast, the L176R mutation led to the destruction of the original hydrogen bond interaction network in CgDAPDH and the formation of a new and more stable hydrogen bond interaction network. In the L176R mutant, the hydrogen bonds were present between Q150, G151, and N270 and pyruvic acid with an occupancy rate of 90%, 90%, and 100%, respectively (Figure 5c). This indicated that pyruvic acid can be stably captured in the binding pocket of L176R, and then remain in a reasonable catalytic

conformation state for a long time, which is consistent with the decreased  $K_m$  value of L176R (Figure 5d). In general, the enhanced amination activity of L176R was primarily attributed to the effective stabilization of the substrate within an optimal catalytic distance in the substrate-binding pocket.

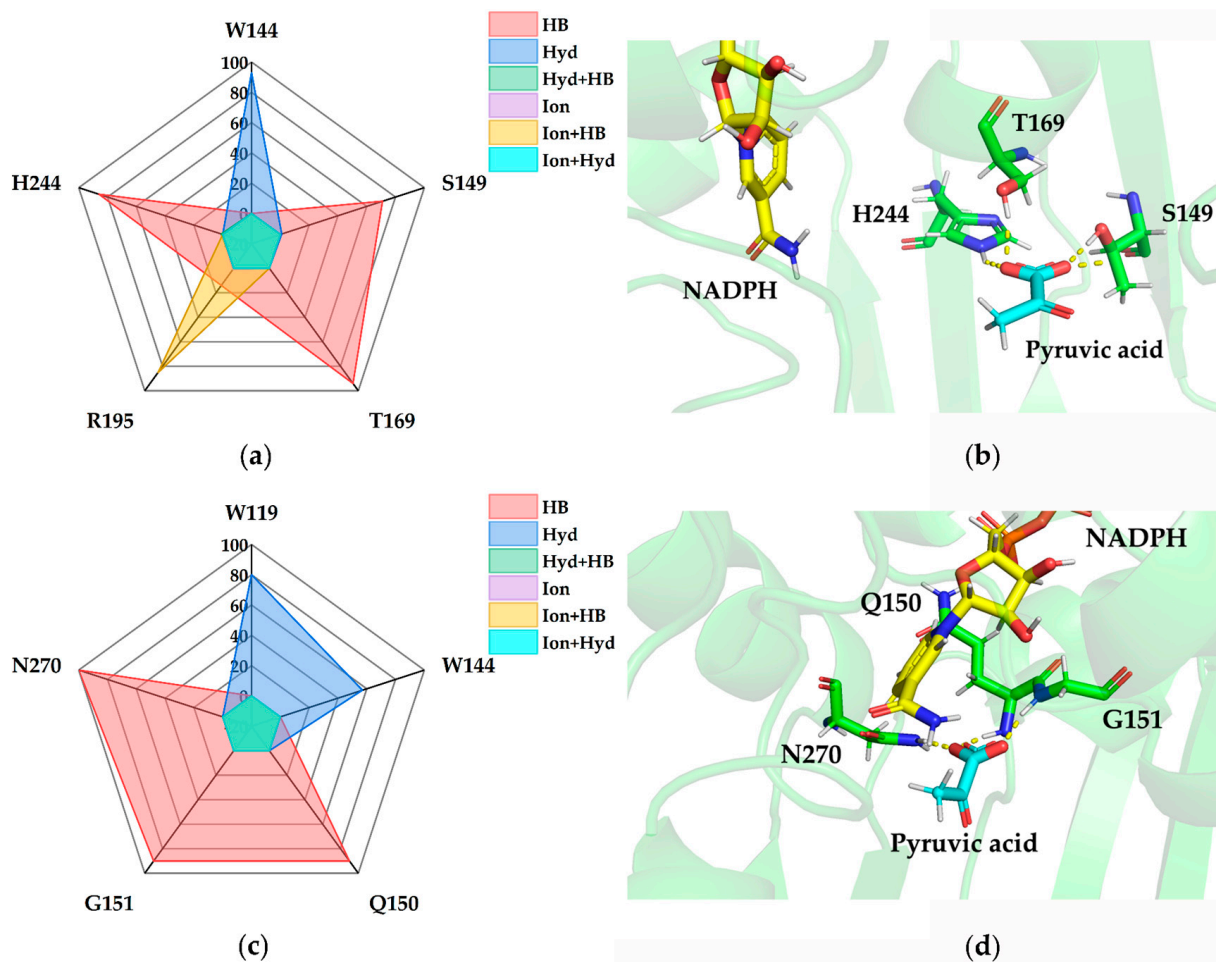


**Figure 5.** Analysis of the interaction force between each residue and pyruvic acid and the binding pocket in the MD simulations: (a) interactions of WT CgDAPDH from the last 20 ns of MD simulations, (b) structure of the pocket of WT CgDAPDH with NADPH, (c) interaction force of the L176R mutant from the last 20 ns of MD simulations and (d) structure of the pocket of the L176R mutant with NADPH. Hydrogen bonds (red), hydrophobic contacts (blue), and ionic interactions (purple); the sum of the hydrogen bonds and hydrophobic contacts [green]; the sum of the ionic interactions and hydrogen bonds (yellow); the sum of ionic interactions and hydrophobic contacts (cyan).

### 3. Discussion

Amino acid sequence alignment between type I and type II has previously demonstrated that the active sites of the two subtypes are highly similar and conserved, with more than 70% of the coenzyme-binding sites highly conserved and consistent [7]. However, type I *meso*-DAPDH shows obvious preference toward *meso*-DAP but almost no amination activity toward 2-keto acids, which is different from type II. By reshaping the interaction force network of amino acids in enzyme proteins, the insertion or deletion of amino acids near the active site can enable enzymes to enhance function or stability [22]. Therefore, based on our previous findings [14], we carried out a systematic study of indels between subtypes targeting the remaining indels in *meso*-DAPDH. Finally, M216, T240, K289, and Q290 were identified as sites that played important roles during the catalysis of CgDAPDH. All of these sites are non-active sites; especially, T240, K289, and Q290 are far from the

substrate-binding domain. More importantly, our DCCM data fully demonstrated that these insertion residues can influence the conformation of the substrate-binding pocket through the interaction force network, which in turn affects the catalytic activity. These four non-active sites were found to be highly dynamic and correlated with other regions of CgDAPDH. Our findings provide a new perspective for the subsequent molecular modification of CgDAPDH that involves considering the effects of non-active sites outside of the active center.

There are limitations associated with the MD simulations used in our study. First, the crystal structures of the alanine mutants used in this study were not known. Amino acid replacement in proteins may lead to conformational changes, which may be localized or affect the overall conformation of the protein. Here, our constructed structure models were based on the crystal structure of WT CgDAPDH, and they may therefore not accurately reflect the conformational changes of the real protein. In addition, although the amino acid residues M216, T240, K289, and Q290 are located on the periphery of the active pocket and away from the dimeric interface, discernible long-range effects have been observed in this study. Consequently, it would be methodologically prudent to conduct simulations incorporating the complete dimeric assembly of CgDAPDH, which requires enormous computational power. Therefore, our results may not fully realize the impact of mutations on the functions of target sites. Future studies will determine the crystal structures of the mutants to allow more accurate and comprehensive analysis of the conformational changes caused by the mutations, as well as their responses to potential inter-subunit crosstalk.

In 2006, Vedha-Peters et al. used CgDAPDH as a template to construct mutant BC621, which was found to produce D-cyclohexylalanine by asymmetric reductive amination of cyclohexyl pyruvate, with an optical purity of more than 99% [5]. In their work, site-directed saturation mutagenesis was first performed with substrate-binding sites as the targets, and then, error-prone PCR was carried out to create mutant libraries. In total, three rounds of mutagenesis were performed, and mutant BC621 was found to contain Arg196Met, Thr170Ile, His245Asn, Gln151Leu, and Asp155Gly [5]. These residues were found to be positioned around the substrate. Our findings prompted our current studies on the sites located beyond the binding pocket in CgDAPDH in an attempt to further understand the molecular mechanism of substrate specificity differences between *meso*-DAPDH subtypes, as well as to carry out protein engineering modifications of CgDAPDH. Our data showing that L176R displayed improved activity toward pyruvic acid highlight the significance of the non-active site L176 in improving its reductive amination activity and demonstrate that it is feasible to understand and engineer *meso*-DAPDH from the perspective of non-active sites. Thus, our results provide an alternative strategy for the subsequent modification of CgDAPDH, which could be applied to other *meso*-DAPDHs.

## 4. Materials and Methods

### 4.1. Materials and Mutant Construction

The recombinant plasmid pET32a(+)-*cgdapdh* was stored in our laboratory. All the experimental materials used here were the same as those reported in our previous study [23].

Using pET32a(+)-*cgdapdh* as a template, alanine mutation was carried out in CgDAPDH using KOD-plus DNA polymerase (TOYOBO, Osaka, Japan) following the site-directed mutagenesis protocol described in our previous study [6]. The mutant libraries of seven amino acid residues including L176, R180, H193, M216, T240, K289, and Q290 were generated by applying oligonucleotide primers containing an NNK degenerate codon at the desired sites [24,25]. All of the mutant libraries were constructed using the PCR-based QuikChange method described previously [6,24]. All the primers are listed in Table S1.

#### 4.2. Screening of Mutant Libraries

Approximately 1300 individual colonies were placed into 96 deep-well plates containing 600  $\mu\text{L}$  of LB medium with 100  $\mu\text{g}/\text{mL}$  ampicillin and incubated at 37  $^{\circ}\text{C}$  for 12 h. For each colony, 200  $\mu\text{L}$  of culture was placed into 96 deep-well plates with fresh LB medium (1 mL per well) and cultured for 2.5–3 h under the same conditions. Seed plates were stored at  $-20^{\circ}\text{C}$  following the addition of glycerol (final concentration of 15%) to each plate. When the  $\text{OD}_{600}$  of the new plate reached 0.6–0.8, the CgDAPDH culture was induced with 0.1 mM isopropyl  $\beta$ -D-thiogalactoside at 37  $^{\circ}\text{C}$  for an additional 6 h. Cell pellets were harvested by centrifugation at 7000 rpm for 10 min, then washed with 200  $\mu\text{L}$  of PB buffer (20 mM, pH 7.4). After full mixing, 100  $\mu\text{L}$  of bacterial solution was taken into a new enzyme-labeled plate. The 0.2 mL of the reaction mixture contained 40  $\mu\text{L}$  of 20 mM pyruvic acid (containing 200 mM  $\text{NH}_4\text{Cl}$ ), 10  $\mu\text{L}$  of 0.5 mM NADPH, and 50  $\mu\text{L}$  of lysozyme mixture with a final concentration of 1 mg/mL and 100  $\mu\text{L}$  of bacterial solution. The reaction mixture was incubated at 30  $^{\circ}\text{C}$  for 12 h. The activity of the supernatant was analyzed using a screening method that detected NADPH consumption. NADPH has a light absorption peak at 340 nm. Thus, the enzyme activity of the mutants can be determined by measuring the consumption of NADPH before and after each sample reaction. An enzymatic reaction was established with pyruvic acid as the screening substrate, and the OD values of each sample were detected at 340 nm before and after the enzymatic reaction using an Epoch2 spectrophotometer (BioTek, Winooski, VT, USA) at 30  $^{\circ}\text{C}$ . Mutants whose OD values decreased significantly after the enzymatic reaction were identified as potential positive mutants. Positive mutants obtained in the screening were used for subsequent purification.

#### 4.3. Protein Expression, Purification, Activity, and Kinetic Parameters

All the proteins, including the WT and variants of CgDAPDH, were overexpressed in *Escherichia coli* BL21(DE3) and purified using Ni-affinity chromatography as described previously [6,7]. The activity assay and kinetic parameters toward *meso*-DAP and pyruvic acid were determined using previously described protocols at 30  $^{\circ}\text{C}$  with an Epoch2 spectrophotometer [14]. Each experiment was performed in triplicate.

#### 4.4. Molecular Dynamic (MD) Simulations

Structural models of the CgDAPDH mutants were generated using the structure of CgDAPDH (PDB ID: 1F06) [4] as a template. Molecular dockings were performed using the YASARA AutoDock VINA [26]. MD simulations of WT CgDAPDH and its mutants were performed using YASARA software 22.5.22 with Amber14 force field [27]. The setup included an optimization of the hydrogen bonding network [28] to increase the solute stability and a pKa prediction to fine-tune the protonation states of the protein residues at the chosen pH of 7.4 [29].  $\text{Na}^+$  and  $\text{Cl}^-$  ions were added at a physiological concentration of 0.9% with an excess of either  $\text{Na}^+$  or  $\text{Cl}^-$  to neutralize the cell. Following steepest-descent and simulated-annealing minimizations to remove clashes, the simulation was run for 50 ns and 100 ns using the AMBER14 force field [30] for the solute, GAFF2 [31] and AM1BCC [32] for the ligands, and TIP3P for water. The cutoff was 8  $\text{\AA}$  for the Van der Waals forces (the default used by AMBER [33]) and no cutoff was applied to the electrostatic forces (using the particle mesh Ewald algorithm [34]). The equations of motion were integrated with a multiple timestep of 1.25 and 2.5 fs for bonded interactions. The simulation system was performed at 298 K and pH 7.4. The RMSD and DCCM for backbone atoms were obtained using YASARA software 22.5.22. The simulation results were visualized using PyMOL software 2.6.0a0 (<https://www.pymol.org>).

## 5. Conclusions

In this study, we generated alanine mutations with CgDAPDH as the template to determine their functions. M216, T240, K289, and Q290 were identified as important residues affecting catalysis. MD analysis showed that the mutations affected the dynamic network of action within the protein and reshaped the substrate-binding pocket. Based on these findings, site-saturation mutagenesis was performed on key indel sites in CgDAPDH, enabling it to efficiently catalyze the reductive amination of pyruvic acid. From seven site-saturation mutant libraries, the optimal mutant CgL176R exhibited a six-fold increase in catalytic efficiency for pyruvic acid compared to WT CgDAPDH. MD analysis revealed that CgL176R formed a more stable catalytic conformation and a hydrogen bond interaction network capable of anchoring pyruvic acid within the binding pocket, thereby positioning it favorably for improved amination activity. Our findings suggest that enhanced amination activity can be effectively achieved by targeting residues away from the active sites.

**Supplementary Materials:** The following supporting information can be downloaded at <https://www.mdpi.com/article/10.3390/catal14040220/s1>, Table S1: Primers used in this study; Figure S1: RMSD analysis of WT CgDAPDH and its alanine mutants MD simulation trajectory; Figure S2: Comparison of substrate-binding energy between WT CgDAPDH and its alanine mutants; Figure S3: Specific activities of WT CgDAPDH and its positive mutants toward pyruvic acid: (a) specific activity of positive mutants at sites L176, R180, H193, and M216; (b) specific activity of positive mutants at sites T240, K289, and Q290. The number after the mutant's name refers to the number on the 96 deep-well plate during the screening process.

**Author Contributions:** Conceptualization, X.G.; methodology, Y.Z. and J.H.; software, Y.Z. and J.H.; validation, Y.Z., Y.C., W.Z. and H.L.; formal analysis, Y.Z. and J.H.; investigation, Y.Z.; resources, Q.M. and X.G.; data curation, Y.Z. and J.H.; writing—original draft preparation, Y.Z. and X.G.; writing—review and editing, X.G.; visualization, Y.Z.; supervision, Q.M. and X.G.; project administration, X.G.; funding acquisition, Q.M. All authors have read and agreed to the published version of the manuscript.

**Funding:** This project was supported by the Natural Science Foundation of Shandong Province (Grant No. ZR2021MC063).

**Data Availability Statement:** Data are contained within this article.

**Acknowledgments:** We thank International Science Editing for editing this manuscript.

**Conflicts of Interest:** The authors declare no conflicts of interest.

## References

1. White, P.J. The essential role of diaminopimelate dehydrogenase in the biosynthesis of lysine by *Bacillus sphaericus*. *J. Gen. Microbiol.* **1983**, *129*, 739–749. [[CrossRef](#)]
2. Misono, H.; Ogasawara, M.; Nagasaki, S. Characterization of *meso*-diaminopimelate dehydrogenase from *Corynebacterium glutamicum* and its distribution in Bacteria (Microbiology & Fermentation Industry). *Agric. Biol. Chem.* **1986**, *50*, 2729–2734.
3. Ishino, S.; Mizukami, T.; Yamaguchi, K.; Katsumata, R.; Araki, K. Nucleotide sequence of the *meso*-diaminopimelate D-dehydrogenase gene from *Corynebacterium glutamicum*. *Nucleic Acids Res.* **1987**, *15*, 3917. [[CrossRef](#)] [[PubMed](#)]
4. Cirilli, M.; Scapin, G.; Sutherland, A.; Vederas, J.C.; Blanchard, J.S. The three-dimensional structure of the ternary complex of *Corynebacterium glutamicum* diaminopimelate dehydrogenase—NADPH-L-2-amino-6-methylene-pimelate. *Protein Sci.* **2000**, *9*, 2034–2037. [[CrossRef](#)]
5. Vedha-Peters, K.; Gunawardana, M.; Rozzell, J.D.; Novick, S.J. Creation of a broad-range and highly stereoselective D-amino acid dehydrogenase for the one-step synthesis of D-amino acids. *J. Am. Chem. Soc.* **2006**, *128*, 10923–10929. [[CrossRef](#)]
6. Gao, X.; Chen, X.; Liu, W.; Feng, J.; Wu, Q.; Hua, L.; Zhu, D. A novel *meso*-Diaminopimelate dehydrogenase from *Symbiobacterium thermophilum*: Overexpression, characterization, and potential for D-amino acid synthesis. *Appl. Environ. Microbiol.* **2012**, *78*, 8595–8600. [[CrossRef](#)]
7. Gao, X.; Zhang, Z.; Zhang, Y.; Li, Y.; Zhu, H.; Wang, S.; Li, C. A newly determined member of the *meso*-diaminopimelate dehydrogenase family with a broad substrate spectrum. *Appl. Environ. Microbiol.* **2017**, *83*, e00476-17. [[CrossRef](#)] [[PubMed](#)]

8. Emond, S.; Petek, M.; Kay, E.J.; Heames, B.; Devenish, S.R.A.; Tokuriki, N.; Hollfelder, F. Accessing unexplored regions of sequence space in directed enzyme evolution via insertion/deletion mutagenesis. *Nat. Commun.* **2020**, *11*, 3469. [[CrossRef](#)]
9. Odokonyero, D.; Sakai, A.; Patskovsky, Y.; Malashkevich, V.N.; Fedorov, A.A.; Bonanno, J.B.; Fedorov, E.V.; Toro, R.; Agarwal, R.; Wang, C.; et al. Loss of quaternary structure is associated with rapid sequence divergence in the OSBS family. *Proc. Natl. Acad. Sci. USA* **2014**, *111*, 8535–8540. [[CrossRef](#)]
10. Hoque, M.A.; Zhang, Y.; Chen, L.; Yang, G.; Khatun, M.A.; Chen, H.; Hao, L.; Feng, Y. Stepwise Loop Insertion Strategy for Active Site Remodeling to Generate Novel Enzyme Functions. *ACS Chem. Biol.* **2017**, *12*, 1188–1193. [[CrossRef](#)]
11. Hashimoto, K.; Panchenko, A.R. Mechanisms of protein oligomerization, the critical role of insertions and deletions in maintaining different oligomeric states. *Proc. Natl. Acad. Sci. USA* **2010**, *107*, 20352–20357. [[CrossRef](#)]
12. Jonas, S.; van Loo, B.; Hyvönen, M.; Hollfelder, F. A new member of the alkaline phosphatase superfamily with a formylglycine nucleophile: Structural and kinetic characterisation of a phosphonate monoester hydrolase/phosphodiesterase from *Rhizobium leguminosarum*. *J. Mol. Biol.* **2008**, *384*, 120–136. [[CrossRef](#)] [[PubMed](#)]
13. Boucher, J.L.; Jacobowitz, J.R.; Beckett, B.C.; Classen, S.; Theobald, D.L. An atomic-resolution view of neofunctionalization in the evolution of apicomplexan lactate dehydrogenases. *eLife* **2014**, *3*, e02304. [[CrossRef](#)] [[PubMed](#)]
14. Ma, Q.; Wang, X.; Luan, F.; Han, P.; Zheng, X.; Yin, Y.; Zhang, X.; Zhang, Y.; Gao, X. Functional Studies on an Indel Loop between the Subtypes of *meso*-Diaminopimelate Dehydrogenase. *ACS Catal.* **2022**, *12*, 7124–7133. [[CrossRef](#)]
15. DuBay, K.H.; Bowman, G.R.; Geissler, P.L. Fluctuations within folded proteins: Implications for thermodynamic and allosteric regulation. *Acc. Chem. Res.* **2015**, *48*, 1098–1105. [[CrossRef](#)]
16. Doshi, U.; Holliday, M.J.; Eisenmesser, E.Z.; Hamelberg, D. Dynamical network of residue-residue contacts reveals coupled allosteric effects in recognition, catalysis, and mutation. *Proc. Natl. Acad. Sci. USA* **2016**, *113*, 4735–4740. [[CrossRef](#)] [[PubMed](#)]
17. Yu, H.; Dalby, P.A. A beginner's guide to molecular dynamics simulations and the identification of cross-correlation networks for enzyme engineering. *Method Enzymol.* **2020**, *643*, 15–49.
18. Sun, Z.; Wu, L.; Bocola, M.; Chan, H.C.S.; Lonsdale, R.; Kong, X.-D.; Yuan, S.; Zhou, J.; Reetz, M.T. Structural and Computational Insight into the Catalytic Mechanism of Limonene Epoxide Hydrolase Mutants in Stereoselective Transformations. *J. Am. Chem. Soc.* **2017**, *140*, 310–318. [[CrossRef](#)] [[PubMed](#)]
19. Li, S.; Cao, L.; Yang, X.; Wu, X.; Xu, S.; Liu, Y. Simultaneously optimizing multiple properties of  $\beta$ -glucosidase Bgl6 using combined (semi-)rational design strategies and investigation of the underlying mechanisms. *Bioresour. Technol.* **2023**, *374*, 128792. [[CrossRef](#)]
20. Wu, K.; Yang, Z.; Meng, X.; Chen, R.; Huang, J.; Shao, L. Engineering an alcohol dehydrogenase with enhanced activity and stereoselectivity toward diaryl ketones: Reduction of steric hindrance and change of the stereocontrol element. *Catal. Sci. Technol.* **2020**, *10*, 1650–1660. [[CrossRef](#)]
21. Ye, W.; Zhang, Y.; Wang, Y.; Xie, J.; Liu, Y.; Yang, L.; Wang, H.; Wei, D. Engineering a Medium-chain Alcohol Dehydrogenase for Efficient Synthesis of (S)-N-Boc-3-pyrrolidinol by Adjusting the Conformational Dynamics of Loops. *ChemCatChem* **2023**, *15*, e202201175. [[CrossRef](#)]
22. Nandwani, N.; Surana, P.; Udgaonkar, J.B.; Das, R.; Gosavi, S. Amino-acid composition after loop deletion drives domain swapping. *Protein Sci.* **2017**, *26*, 1994–2002. [[CrossRef](#)]
23. Gao, X.; Ma, Q.; Chen, M.; Dong, M.; Pu, Z.; Zhang, X.; Song, Y. Insight into the Highly Conserved and Differentiated Cofactor-Binding Sites of *meso*-Diaminopimelate Dehydrogenase StDAPDH. *J. Chem. Inf. Model.* **2019**, *59*, 2331–2338. [[CrossRef](#)]
24. Hogrefe, H.H.; Cline, J.; Youngblood, G.L.; Allen, R.M. Creating randomized amino acid libraries with the QuikChange® Multi Site-Directed Mutagenesis Kit. *Biotechniques* **2002**, *33*, 1158–1165. [[CrossRef](#)] [[PubMed](#)]
25. Zheng, L.; Baumann, U.; Reymond, J.L. An efficient one-step site-directed and site-saturation mutagenesis protocol. *Nucleic Acids Res.* **2004**, *32*, e115. [[CrossRef](#)] [[PubMed](#)]
26. Trott, O.; Olson, A.J. AutoDock VINA: Improving the speed and accuracy of docking with a new scoring function, efficient optimization and multithreading. *J. Comput. Chem.* **2009**, *31*, 455–461. [[CrossRef](#)] [[PubMed](#)]
27. Krieger, E.; Vriend, G. New ways to boost molecular dynamics simulations. *J. Comput. Chem.* **2015**, *36*, 996–1007. [[CrossRef](#)] [[PubMed](#)]
28. Krieger, E.; Dunbrack, R.L., Jr.; Hooft, R.W.; Krieger, B. Assignment of protonation states in proteins and ligands: Combining pKa prediction with hydrogen bonding network optimization. *Methods Mol. Biol.* **2012**, *819*, 405–421. [[PubMed](#)]
29. Krieger, E.; Nielsen, J.E.; Spronk, C.A.; Vriend, G. Fast empirical pKa prediction by Ewald summation. *J. Mol. Graph. Model.* **2006**, *25*, 481–486. [[CrossRef](#)]
30. Maier, J.A.; Martinez, C.; Kasavajhala, K.; Wickstrom, L.; Hauser, K.E.; Simmerling, C. ff14SB: Improving the Accuracy of Protein Side Chain and Backbone Parameters from ff99SB. *J. Chem. Theory Comput.* **2015**, *11*, 3696–3713. [[CrossRef](#)]
31. Wang, J.; Wolf, R.M.; Caldwell, J.W.; Kollman, P.A.; Case, D.A. Development and testing of a general amber force field. *J. Comput. Chem.* **2004**, *25*, 1157–1174. [[CrossRef](#)] [[PubMed](#)]
32. Jakalian, A.; Jack, D.B.; Bayly, C.I. Fast, efficient generation of high-quality atomic charges. AM1-BCC model: II. Parameterization and validation. *J. Comput. Chem.* **2002**, *23*, 1623–1641. [[CrossRef](#)] [[PubMed](#)]

33. Hornak, V.; Abel, R.; Okur, A.; Strockbine, B.; Roitberg, A.; Simmerling, C. Comparison of multiple Amber force fields and development of improved protein backbone parameters. *Proteins* **2006**, *65*, 712–725. [[CrossRef](#)] [[PubMed](#)]
34. Essmann, U.; Perera, L.; Berkowitz, M.L.; Darden, T.; Lee, H.; Pedersen, L.G. A smooth particle mesh Ewald method. *Chem. Phys.* **1995**, *103*, 8577–8593. [[CrossRef](#)]

**Disclaimer/Publisher’s Note:** The statements, opinions and data contained in all publications are solely those of the individual author(s) and contributor(s) and not of MDPI and/or the editor(s). MDPI and/or the editor(s) disclaim responsibility for any injury to people or property resulting from any ideas, methods, instructions or products referred to in the content.